Composite Structures 143 (2016) 362–370

Contents lists available at ScienceDirect

Composite Structures

journal homepage: www.elsevier.com/locate/compstruct

Design and characterisation of advanced pseudo-ductile unidirectional thin-ply carbon/epoxy–glass/epoxy hybrid composites

Gergely Czél [a,b,*], Meisam Jalalvand [b], Michael R. Wisnom [b]

[a] MTA–BME Research Group for Composite Science and Technology, Budapest University of Technology and Economics, Műegyetem rkp. 3., H-1111 Budapest, Hungary
[b] Advanced Composites Centre for Innovation and Science, University of Bristol, Queen's Building, BS8 1TR Bristol, United Kingdom

ARTICLE INFO

Article history:
Available online 9 February 2016

Keywords:
Pseudo-ductility
Thin-ply composites
Fragmentation
Delamination
Damage and fracture mechanics
Mechanical testing

ABSTRACT

A comprehensive set of thin-ply pseudo-ductile unidirectional interlayer hybrid composite materials comprising S-glass and a variety of thin carbon prepregs was designed and characterised. Unique elastic–yielding–hardening type stress–strain responses similar to those of ductile metals were achieved through fragmentation and stable pull-out of the carbon layers, generating a range of initial moduli, pseudo-yield strains, plateau stresses and pseudo ductile strains for the various configurations. The typical failure modes of thin-ply hybrid composites were highlighted in four series of stress–strain graphs obtained for the same materials with different carbon layer thicknesses. The predicted failure modes agreed well with the experimental results and demonstrated the merit of our two step design framework based on (i) simple analytical criteria and (ii) novel damage mode maps.

1. Introduction

High performance fibre reinforced composites offer outstanding strength and stiffness together with low density, therefore they are traditionally considered for advanced lightweight applications such as aero-structures, spacecraft, motorsports, high specification sports equipment, etc. However, their relatively high material and manufacturing cost and their usually brittle, catastrophic failure without sufficient warning restricts their spread towards many high volume applications including mass produced automotive and construction, where unexpected failure and poor residual integrity cannot be tolerated. The unfavourable failure characteristic is usually compensated for by conservative design limits, which hinders component manufacturers from fully exploiting the excellent mechanical properties of composites. High performance ductile or pseudo-ductile composites delivering safe failure mechanisms similar to metals' yielding and strain hardening with detectable warning and a wide margin before final failure are therefore of significant interest.

Adding ductility as a new feature to composite materials is particularly challenging because both traditional constituents of high performance long fibre reinforced thermoset polymer matrix composites (i.e. fibres such as glass, carbon and thermosetting resins such as epoxy, unsaturated polyester) are intrinsically brittle [1]. Modified matrix systems including hybrid resins [2] can only provide a small increase in properties such as impact and fatigue resistance because the mechanical response of composites is usually fibre dominated.

Development of new ductile fibres is challenging although nanotube fibre spinning seems promising [3] but it is a long process to verify and commercialise a new fibre. Ductile steel fibres have also been investigated as reinforcement for composites especially after low diameter filaments of high performance annealed stainless steel emerged recently. Excellent ductility with tensile failure strains well beyond 10% was reported [4–7]. The trade-off for high failure strains and ductile failure in these composites seems to be their high density and moderate performance compared to carbon/epoxy.

An alternative approach is to modify the architecture of traditional laminated composites e.g. by generating additional strain through the realignment of off-axis fibres [8–10] or out of plane waviness [11], which can generate extra strain before failure by allowing reorientation of the fibres. Interface modification on the fibre [12] and on the ply level [13] as well as designed discontinuities [14,15] are also suitable for delaying fracture and generating non-linearity through controlled damage before final failure. Hybridisation of commercially available unidirectional (UD) plies is another approach to maintain high initial modulus and potentially introduce a gradual failure, although it usually results in

* Corresponding author at: MTA–BME Research Group for Composite Science and Technology, Budapest University of Technology and Economics, Műegyetem rkp. 3., H-1111 Budapest, Hungary. Tel.: +36 14631462; fax: +36 14631527.
E-mail address: czel@pt.bme.hu (G. Czél).

http://dx.doi.org/10.1016/j.compstruct.2016.02.010
0263-8223/

unfavourable major load drops when the lower strain fibres break. Our intention is to address this issue and fully exploit the benefits of hybridisation for progressive, pseudo-ductile failure.

Intensive research on hybrid composites typically containing glass and carbon fibres was initiated early in the 1970s and focussed on improving the low strain and brittle failure of early carbon composites. A few review papers summarised the structure and properties of the hybrids studied over the first decades [16–20]. Good potential for improving the brittle failure of single fibre type composites was reported with two major approaches: (i) interlayer or ply-by-ply hybrids [21–24] and (ii) intimately mixed or intermingled hybrids [25,26]. A more recent review by Swolfs et al. [27] pointed out the potential for adding pseudo-ductility to high performance composites as an emerging field for hybrid composites. Intermingling of continuous fibres proved to be challenging and only moderate degree of dispersion has been reported using productive continuous technologies such as tow spreading [28]. On the other hand, very promising results were presented recently by Yu et al. with a new technique to manufacture highly aligned short fibre composites [29] and well dispersed intermingled short fibre hybrids [30], which showed pseudo-ductile failure. In this study we focussed on interlayer hybrids, which are simpler to manufacture by stacking layers of different prepregs together. The potential for achieving pseudo-ductility was demonstrated earlier by the authors [31,32] using standard thickness E-glass and emerging thin-ply carbon prepregs suitable for suppressing unstable delamination in UD interlayer hybrid composites during and after the fragmentation of the low strain material of the hybrid. Although the initial results were promising, the extent of pseudo-ductile strains was moderate because of the limited glass/epoxy strength.

The recently introduced thin ply composites have generated high interest and have been studied extensively [33–42] because of their unique potential to allow for highly dispersed lay-up designs which results in favourable damage suppression properties. The general conclusion of the cited studies is that the onset of damage is delayed and the strength is usually increased in unnotched thin-ply composites because premature matrix cracking and delamination can be suppressed due to the lower energy release rates with thin plies, but the final failure in return becomes more brittle. Thin carbon layers in interlayer hybrids on the contrary show favourable progressive damage (i.e. fragmentation) by suppressing unstable delamination after the first carbon layer fracture in a glass–carbon hybrid laminate due to low energy released [31]. The unique, so-called stable pull-out damage type refers to the stable delamination of the carbon layer fragments from the undamaged glass layers. Stable pull-out takes place after the onset of carbon layer fragmentation, but well before final failure and therefore it is a key enabling damage mechanism of pseudo-ductile thin-ply UD hybrid composites together with fragmentation.

The aim of this research is to develop a set of immediately applicable pseudo-ductile composite materials exploiting the demonstrated thin-ply hybrid concept [31], the recently developed analytical modelling and design tools [43,44] and a comprehensive new set of constituent materials with a wide range of properties. The developed new UD pseudo-ductile composites are expected to be suitable for some specific applications where tensile loading is highly dominant and also provide a strong foundation for further development of more versatile pseudo-ductile materials.

2. Material and configuration design

This section gives details of the overall concept, the applied materials and the design considerations to assure a stable pseudo-ductile failure of the hybrid laminates.

2.1. Concept

Thin-ply UD interlayer hybrid composites have recently demonstrated the potential for pseudo-ductility [31] through fragmentation and stable pull-out of a *low strain* (carbon) *layer* in the centre of the laminate from the outer *high strain* (glass) *layers*. In addition, the hybrid composites have about 5% lower density and typically minimum 20% higher initial modulus than the baseline glass/epoxy. However in the demonstration phase of the research, standard E-glass was applied for the high strain layers, which did not have a high enough strain margin especially when hybridised with high strength carbon fibres, therefore no increase in stress was achieved after pseudo-yielding (after the knee point marked with (1) on Fig. 1). Advanced design tools, higher performance S-glass and a variety of the available thin carbon prepregs were utilised in the present study resulting in a range of pseudo-ductile responses, with wide stress and strain margins between the initiation of damage and final failure. Fig. 1 shows the expected stress–strain response and the typical appearance of a UD thin-ply interlayer glass/carbon hybrid composite specimen at successive damage phases (carbon fragmentation and stable pull-out). The key feature of the expected response compared with our previous results which offered a relatively short, flat stress plateau, is the second rising part after a much longer plateau. This beneficial extra feature is achievable with advanced high strength S-glass prepregs, which can provide a stress margin and extended strain margin before final failure.

2.2. Materials

The set of available thin-ply UD prepreg materials was found to be very limited. Therefore the design of the configurations was significantly limited by material availability especially by the lack of thin S-glass in a tough epoxy matrix. The materials considered for design, and used for the experiments were standard thickness S-glass/epoxy prepregs supplied by Hexcel, thin S3-glass/epoxy from North Thin Ply Technology and various thin carbon/epoxy prepregs from SK Chemicals and North TPT. The epoxy resin systems in the prepregs were the aerospace grade 913 (Hexcel), ThinPreg 120 EPHTg-402 (North TPT) and K50 (SK chemicals). All resins in the hybrid laminates were 120 °C cure epoxies, which were found to be compatible, although no details were provided by the suppliers on the chemical formulation of the resins. Good integrity of the hybrid laminates was confirmed during test procedures and no phase separation was observed on cross sectional micrographs. Basic properties of the applied fibres and prepreg systems can be found in Tables 1 and 2.

2.3. Design of hybrid laminates

The following design criteria were identified and published earlier [31] to assure stable pseudo-ductile failure for UD glass/carbon interlayer hybrids. These criteria were adopted here for the preliminary design of similar interlayer hybrid configurations with new sets of constituent prepregs:

(i) The outer, high strain layers need to be thick and strong enough to take the full load after low strain material fracture and pull-out with a sufficient margin. This is required to account for stress concentration in the glass layer due to the carbon layer fracture which is not considered in this approach, but shown to be moderate for similar interlayer hybrid configurations [43]. Formula (1) gives the minimum strength of the high strain layer for given layer thicknesses and initial moduli, which is usually determined by the available prepreg types.

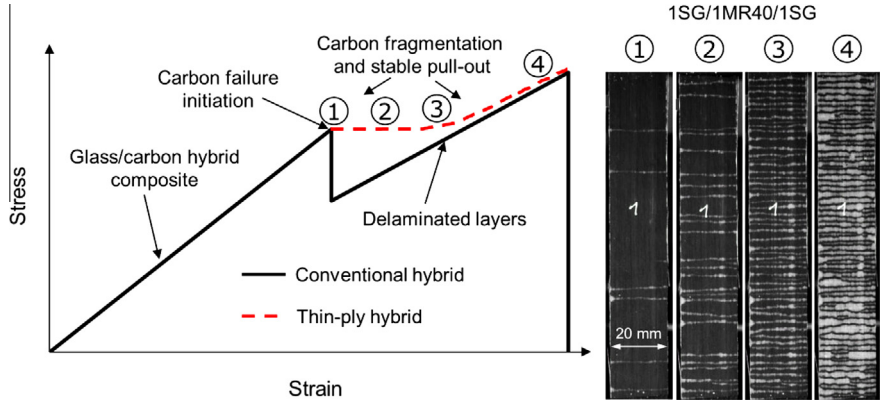

Fig. 1. Schematic of the stress–strain response of conventional and thin-ply interlayer hybrid composites and typical appearance of thin-ply hybrid specimens at successive damage phases (dark areas show bonded, light areas show damaged glass/carbon interface through the translucent outer glass layer).

Table 1
Fibre properties of the applied UD prepregs based on manufacturer's data (carbon fibre types: SM – standard modulus, IM – intermediate modulus, HM – high modulus and UHM – ultra-high modulus).

Fibre type	Manufacturer	Tensile modulus [GPa]	Strain to failure [%]	Tensile strength [GPa]	Density [g/cm^3]
Pyrofil TR30 carbon	Mitsubishi Rayon	234 (SM)	1.9	4.41	1790
Pyrofil MR40 carbon	Mitsubishi Rayon	295 (IM)	1.5	4.41	1760
Pyrofil HS40 carbon	Mitsubishi Rayon	455 (HM)	1.0	4.61	1850
Torayca T1000 carbon	Toray	294 (IM)	2.2	6.37	1800
Torayaca M55JB carbon	Toray	540 (HM)	0.8	4.02	1910
Granoc XN80 carbon	Nippon GFC	780 (UHM)	0.5	3.43	2170
S3 UHM glass	AGY advanced materials	99	–	3.30	2830
FliteStrand S ZT S-glass	Owens corning	88	5.5	4.8–5.1	2450

Table 2
Cured ply properties of the applied UD prepregs.

Prepreg material	Manufacturer	Fibre areal mass[a] [g/m^2]	Cured ply thickness[b] [μm]	Fibre volume fraction[a] [%]	Initial modulus[b] [GPa]
TR30/epoxy	SK chemicals	21 [31]	28.9 [31]	41 [31]	101.7 [8]
MR40/epoxy	SK chemicals	50	61.4	45	134.6
HS40/epoxy	SK chemicals	65	70.3	50	229.2
T1000/epoxy	North TPT	28	32.3	48	143.3
M55/epoxy	North TPT	30	30.5	52	280.0
XN80/epoxy	North TPT	50	50.5	46	357.5
S3-glass/epoxy	North TPT	85	49.2	61	61.7
S-glass/epoxy	Hexcel	190	155.1	51	45.6 [45]

Values with references were determined experimentally by our group previously.
[a] Based on manufacturer's datasheet.
[b] Calculated using manufacturer's data.

$$\sigma_{1b} > \frac{\sigma_{2b}(2E_1t_1 + E_2t_2)}{2E_2t_1} \quad (1)$$

where E_1 is the initial modulus of the high strain (glass) layers, E_2 is the initial modulus of the low strain (carbon) layer, t_1 is the thickness of one high strain layer, t_2 is the thickness of the low strain layer as shown on Fig. 3, σ_{1b} is the breaking stress of the high strain layers, σ_{2b} is the breaking stress of the low strain layer.

(ii) The energy release rate (G_{II}) at the expected failure strain of the low strain (carbon) layer must be lower than the mode *II* fracture toughness (G_{IIC}) of the interface to avoid delamination of the central low strain layer after its first fracture. This criterion assures the condition for the multiple fractures (i.e. fragmentation) and stable pull-out of the low strain layer.

$$G_{IIC} > G_{II} = \frac{\varepsilon_{2b}^2 E_2 t_2 (2E_1t_1 + E_2t_2)}{8E_1t_1} \quad (2)$$

where ε_{2b} is the failure strain of the low strain layer.

The preliminary design resulted in the material configurations summarised in Table 3. The fracture toughness (G_{IIC}) of the glass/-carbon composite interface was measured earlier in [46] for UD E-glass/TR30 carbon hybrid specimens, where the central carbon plies were cut perpendicular to the fibres before lay-up and curing. The hybrid specimens were made with the same 913 resin in the E-glass prepreg as that in the S-glass prepreg applied in this study. Based on our previous results obtained from specimens comprising the same resin in the glass prepregs, 1.0 N/mm was used as an estimated G_{IIC} for all S-glass configurations. A lower G_{IIC} value was assumed for the S3G/M55/S3G configuration where the S3-glass prepreg was made with North TPT's resin which exhibited lower toughness during the tests of similar interlayer hybrids of other materials comprising the same resin system. A change from stable to unstable failure was observed in configurations having G_{II} >

Table 3
Specimen types tested within the present study (specimen type designation: SG-S-glass, S3G-S3-glass. Subscripts indicating the number of plies in a block are only added where multiple plies are stacked together. Relative carbon layer thickness was normalised with the full specimen thickness).

Spec. Type	Fibre areal mass [g/m^2]	Nominal thickness [mm]	Relative carbon layer thickness [–]	Calculated G_{II} at carbon fibre failure strain [N/mm]	Approx. G_{IIC} [N/mm]
SG/TR30/SG	190/21/190	0.339	0.085	0.306 at 1.9%	1
SG/TR30$_2$/SG	190/42/190	0.368	0.157	0.715 at 1.9%	1
SG/TR30$_3$/SG	190/63/190	0.397	0.218	1.225 at 1.9%	1
SG$_2$/TR30$_4$/SG$_2$	380/84/380	0.736	0.157	1.430 at 1.9%	1
SG/MR40/SG	190/50/190	0.372	0.165	0.736 at 1.5%	1
SG/HS40/SG	190/65/190	0.381	0.185	0.861 at 1%	1
SG$_2$/HS40/SG$_2$	380/69/380	0.691	0.102	0.632 at 1%	1
SG/T1000/SG	190/28/190	0.343	0.094	0.744 at 2.2%	1
S3G/M55/S3G	85/30/85	0.129	0.236	0.328 at 0.8%	0.5
SG/XN80$_2$/SG	190/100/190	0.411	0.246	0.802 at 0.5%	1

0.5 N/mm therefore this value was adopted as an approximation for G_{IIC}. Most of the predicted G_{II} energy release rates in the table are lower than the critical value (G_{IIC}), therefore stable, pseudo-ductile failure is expected for these specimen types. The two configurations with three and four TR30 carbon layers (the one with four TR30 plies is a scaled version of the one with two TR30 plies) have energy release rates higher than the estimated fracture toughness of the carbon/glass layer interfaces and so were not expected to show pseudo-ductility. These were tested to confirm the assumed energy release rate values and presented to give a more comprehensive set of failure behaviours of UD interlayer hybrids.

A novel representation of the damage modes of interlayer hybrid composites developed recently by the authors [43,44] was applied to the tested configurations of this study and presented in Fig. 2 to show their expected damage modes. Each map divides all possible configurations of a material pair into four groups associated with four possible damage sequences of UD interlayer hybrid composites i.e. (1) premature glass failure: the whole hybrid specimen fails at first carbon fracture, (2) unstable delamination: the layers delaminate at first carbon fracture, (3) carbon layer fragmentation: the energy released at first carbon layer fracture is not enough to drive unstable delamination, so other fractures take place in the carbon layer until they saturate, (4) carbon fragmentation and stable delamination: the energy release rate exceeds the critical value before final failure, therefore the fragmented carbon segments are pulled-out stably from the glass layers. The maps can easily be used as a design tool to achieve optimal hybrids with desired damage modes. Full details of the possible damage scenarios and the construction of the maps can be found in [43,44].

Each damage mode map in Fig. 2 has four regions with the expected damage modes explained briefly in Fig. 2f. The horizontal axis of each map shows the carbon layer thickness relative to the full thickness and the vertical one shows the absolute thickness of the carbon layer so every point on the map represents a specific hybrid configuration. The maps show the expected damage modes and the achievable pseudo-ductile strains for the selected configurations marked with circles. The coloured regions of the map indicate favourable pseudo-ductile damage process and the white regions show either premature glass layer failure or catastrophic delamination. The pseudo-ductile strain is defined between a point at the initial slope line at failure stress and the final failure strain as shown in Table 4.

Each damage mode map in Fig. 2 was generated assuming a G_{IIC} = 1 N/mm fracture toughness (except for the S3-glass/M55 configuration with G_{IIC} = 0.5 N/mm) and the first carbon layer fracture at the failure strain of the corresponding constituent fibres (see Table 1).

The glass layer failure was predicted using a statistical strength distribution based on the fibre failure strain and typical Weibull parameters for glass fibres. Stress concentrations around the fractured low strain layer were taken into account as explained in [43], but those at the end-tab region were not considered, therefore the predicted pseudo-ductile strains represent upper bounds.

Eight of the ten different configurations marked with circles on the damage mode maps are expected to fail in a stable pseudo-ductile way while the remaining two S-glass/TR30 configurations with thick carbon layers are included in Fig. 2a for completeness only. The majority of the pseudo-ductile configurations fall into the most advantageous region (4) (carbon layer fragmentation + stable pull-out), where the highest pseudo-ductile strain can be achieved. Only the SG/TR30/SG configuration is at the border of regions (3) and (4) in Fig. 2a, therefore there is a risk of limited pseudo-ductile strain here, because only fragmentation, but no stable delamination is predicted. If there is no stable delamination around a crack in the carbon layer, the stiffness reduction will be minor, and a high stress-concentration may arise and break the surrounding glass layers resulting in the final failure of the whole specimen earlier than in a stably delaminating configuration.

3. Experimental

3.1. Specimen geometry

The specimens tested within the experimental part of the study were UD, parallel edge tensile specimens. Nominal specimen dimensions were 240/160/20/h mm overall length/L_f-free length/W-width/h-variable thickness respectively. Fig. 3 shows the geometric parameters on the side and top view schematics of a tensile specimen.

3.2. Specimen manufacturing

The interlayer hybrid specimens were made by stacking the specified prepreg layers on top of each other, vacuum bagging the composite plate and curing it in an autoclave according to the longest of the recommended cure cycles of the constituent prepregs at their common 120 °C cure temperature and 0.7 MPa pressure. The individual specimens were fabricated with a diamond cutting wheel. Finally 40 mm long cross-ply glass/epoxy tabs were bonded to the ends of the specimens.

3.3. Test method

Testing of the parallel edge specimens was executed under uniaxial tensile loading and displacement control at a crosshead speed of 2 mm/min on a computer controlled Instron 8801 type 100 kN

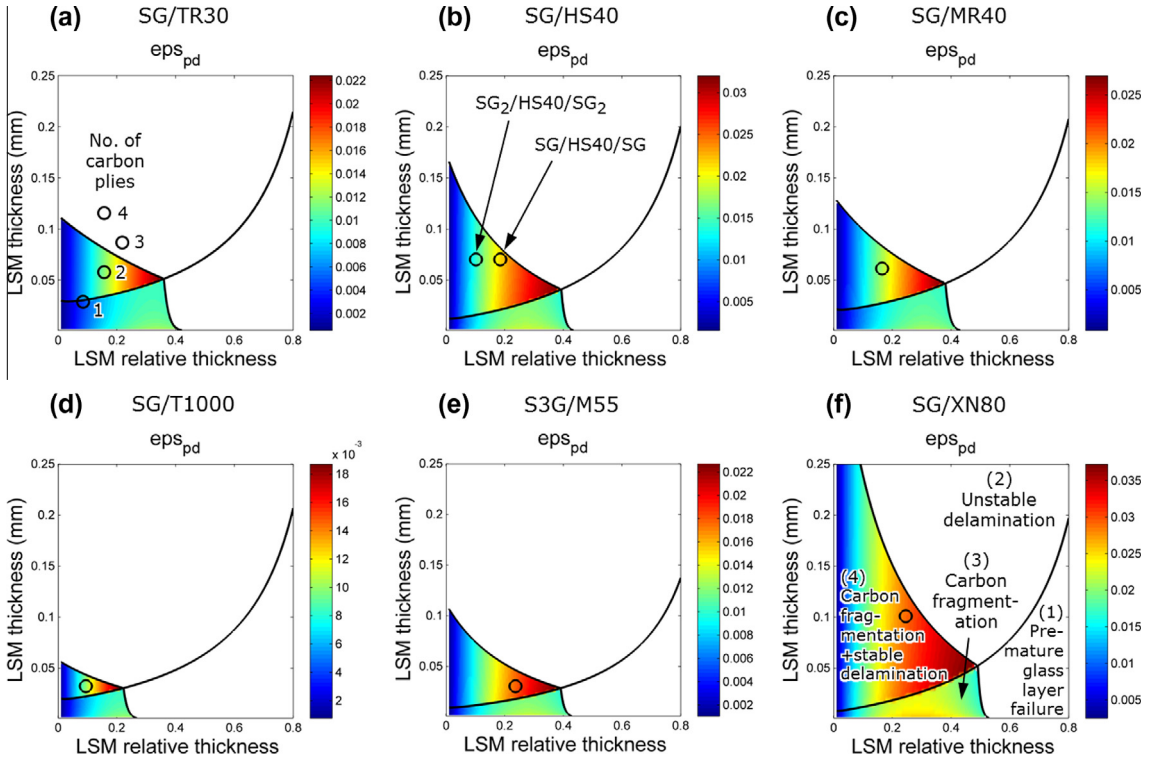

Fig. 2. Damage mode maps of the designed material combinations with S-glass and various carbon plies (eps_{pd} – pseudo-ductile strain, LSM – low strain material (i.e. carbon), part f) indicates four regions of the map with their associated failure processes).

Table 4
Results summary of the specimen types tested (specimen type designation: SG-S-glass, S3G-S3-glass. Relative carbon layer thickness was normalised with the full specimen thickness. Numbers in brackets indicate the coefficients of variation in [%]).

Spec. Type	Relative carbon layer thickness	Initial modulus	Modulus increase (to pure glass/epoxy[a])	Pseudo-yield/drop strain[b]	Pseudo-yield/plateau stress[b]	Approx. final failure strain	Pseudo-ductile strain[c]
	[-]	[GPa]	[%]	[%]	[MPa]	[%]	[%]
SG/TR30/SG	0.0852	50.18 (2.2)	9.98	2.38	1142	3.7	0.91
SG/TR30$_2$/SG	0.1570	53.36 (3.6)	16.94	2.21	1129	3.4	1.21
SG/TR30$_3$/SG	0.2184	56.76 (1.3)	24.40	1.86	-	3.5	-
SG$_2$/TR30$_4$/SG$_2$	0.1570	53.40 (1.2)	17.03	1.90	-	3.7	-
SG/MR40/SG	0.1652	59.89 (2.0)	31.26	1.72	972	3.5	1.44
SG/HS40/SG	0.1847	78.59 (2.9)	72.24	1.11[d]	893[e]	3.7	2.12[e]
SG$_2$/HS40/SG$_2$	0.1017	65.12 (1.0)	42.71	1.28	768	3.7	1.64
SG/T1000/SG	0.0943	54.21 (1.1)	18.81	2.61	1358	3.4	0.80
S3G/M55/S3G	0.2364	112.89 (4.3)	82.97	0.85	852	3.0	2.06
SG/XN80$_2$/SG	0.2457	124.14 (6.4)	172.07	0.52	520	3.6	2.64

[a]Baseline S-glass composite modulus: 45.6 GPa (see Table 2)
[b]*Pseudo-yield points* were defined as the intersection of the test curve with a straight line parallel to the initial slope of the stress-strain graph with an offset of 0.1% strain (similar to the offset yield point or proof stress in metals terminology).
[c]*Pseudo-ductile strain* was defined between the strain of a point on the initial slope line at the *failure stress* (defined at the point where a 5% reduction in stress after the maximum has occurred) and the *strain at the failure stress*.
[d]Determined at first load drop
[e]Load drops observed on the plateau (see Fig. 5)

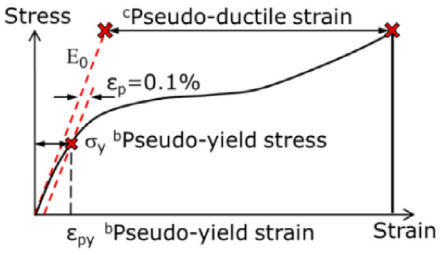

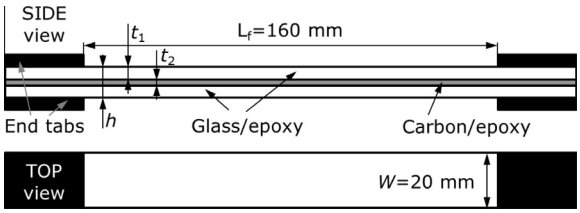

Fig. 3. Schematic of the specimen geometry.

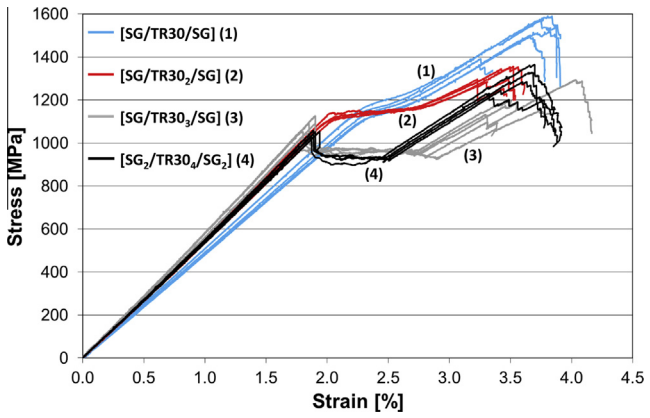

Fig. 4. Tensile stress–strain graphs of S-glass/TR30 carbon configurations.

rated universal hydraulic test machine with a regularly calibrated 25 kN load cell and wedge type hydraulic grips. Strains were measured using an Imetrum videogauge system, with a nominal gauge length of 130 mm. A minimum of five specimens were tested from each configuration.

3.4. Results and discussion

Fig. 4 shows the stress–strain response of all four configurations comprising high strength (standard modulus) TR30 carbon plies. The thinnest specimens made with only one thin carbon ply had a low relative carbon layer thickness, therefore relatively low initial modulus and moderate decrease in the slope of the final rising part of the stress–strain curves was observed. Short plateaus in between the successive quasi-linear parts of the curve and smooth transitions between them were observed, which suggest a very dispersed, fragmentation dominated failure, where several short cracks develop in parallel, instead of larger ones running across the whole specimen width. This fragmentation mechanism was confirmed by the observed narrow, non-straight cracks, which appeared in the carbon ply just before the first smooth knee (between 2% and 2.5% strain) in the curve. These cracks were visible through the translucent glass ply, while growing simultaneously and gradually covering the whole specimen with an approx. 1 mm spacing. This slow damage accumulation and the corresponding limited pseudo-ductility is in agreement with the predicted damage mode (Fig. 2a). The reason for the observed benign damage accumulation is the low G_{II} of this configuration due to the very low carbon layer thickness.

The SG/TR30$_2$/SG configuration showed a favourable pseudo-ductile failure producing a pronounced knee around the failure strain of the carbon, which can be interpreted as *pseudo-yielding*. A wide, slightly rising plateau and finally a second rising part can be observed on the stress–strain graph, providing sufficient stress margin after the first failure event before final failure. The specimens showed a striped pattern with an average spacing of around 2–3 mm due to the well predicted fragmentation resulting in long, straight cracks typically across the whole specimen width and stable pull-out of the carbon layer fragments (see Fig. 2a). The initial modulus of this configuration was significantly higher than that of the single ply one due to the higher relative carbon layer thickness.

The SG/TR30$_3$/SG and the SG$_2$/TR30$_4$/SG$_2$ configurations showed load drops, which rendered them unsuitable for pseudo-ductility, but the test results were consistent with our expectations based on the calculated energy release rates included in Table 3. Both specimen types delaminated to a certain extent (~30–50 mm) immediately after the first fracture in the carbon layer, as predicted by the damage mode map (Fig. 2a), and then the pull-out of the carbon layer continued stably indicated by the flat parts of the graphs after the load drops. Fig. 4 demonstrates the significant difference in the behaviour of the same hybrid material combination due to an increase from two to three thin central carbon plies. The reason is that three carbon plies released enough energy to delaminate the layers at the first carbon fracture, while the pull-out of two plies remained stable. The completely different graphs of the two scaled thickness specimen types SG/TR30$_2$/SG and SG$_2$/TR30$_4$/SG$_2$ also highlight the effect of ply thickness in interlayer hybrid composites. It is also interesting to note, that the first knee of the curves corresponding to the carbon layer failure strain was shifted significantly towards higher strains if thin central layers were incorporated. This is attributed to the hybrid effect which is discussed in [47]. Fig. 4 reveals that the "width" of the pseudo-ductile stress plateau as well as the initial modulus of the hybrid material is controlled by the relative carbon layer thickness, while the failure type is strongly affected by the absolute thickness of the carbon layer (through G_{II}) for a given glass thickness (see the configurations with 1–3 carbon plies).

Fig. 5 shows the stress–strain graphs of two configurations comprising high modulus HS40 carbon prepreg. Favourable pseudo-ductile behaviour was predicted for both configurations through the damage mode maps in Fig. 2b although the thinner laminate was close to the upper boundary of region (4) due to having the highest sub-critical energy release rate of all tested specimen types at the carbon layer failure strain (Table 3). Furthermore, the test results indicated that the average strain at the first fracture of the carbon layer (accompanied by a minor load drop) was significantly higher (around 1.1%) than that quoted by the fibre manufacturer (1%). An updated energy release rate calculation using the experimental carbon layer failure strain yielded an energy release rate G_{II} = 1.04 N/mm right at the limit for delamination. The small load-drops on the stress–strain graphs were observed during the tests to correspond to successive limited delaminations immediately after each carbon layer fragmentation.

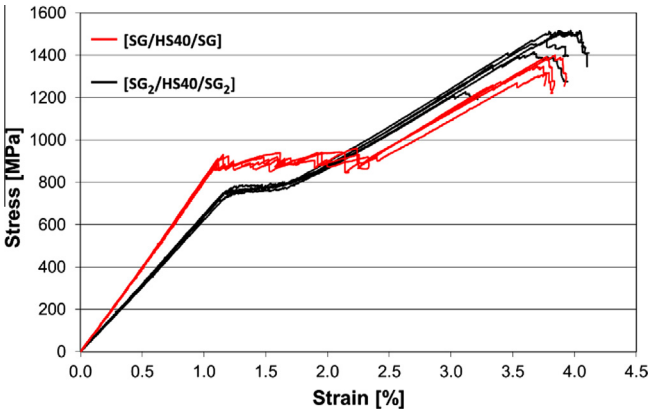

Fig. 5. Tensile stress–strain graphs of S-glass/HS40 carbon configurations.

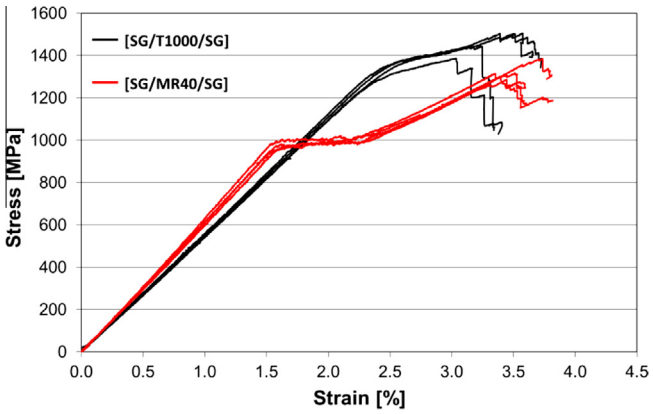

Fig. 6. Tensile stress–strain graphs of S-glass/IM carbon configurations.

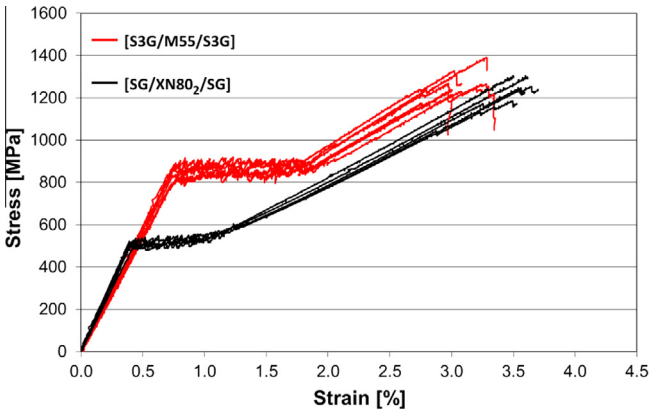

Fig. 7. Tensile stress–strain graphs of S-glass/HM and UHM carbon configurations.

The overall behaviour of the SG/HS40/SG configuration is very attractive with high initial modulus (up to 75% higher than that of UD S-glass/epoxy) and a 1% strain wide plateau, therefore it was developed further in [45] with a special architecture where the carbon ply was periodically cut perpendicular to the fibre direction to initiate stable pull out and avoid delamination. The thicker $SG_2/HS40/SG_2$ configuration had a lower energy release rate (G_{II} = 0.835 N/mm) even though it was updated with the experimentally observed 1.15% strain for carbon fracture. This configuration therefore showed a stable, pseudo-ductile failure, but a shorter plateau and decreased initial modulus, due to the relatively low carbon proportion. A slightly thinner carbon ply could have been beneficial for this material combination but our material choice was limited.

Fig. 6 shows the results of configurations made with intermediate modulus carbon fibres, both showing favourable pseudo-ductile stress strain responses in agreement with their damage-mode maps (Fig. 2c and d). The key difference between the similar modulus carbon fibre types applied, was their failure strain. The very high failure strain of T1000 fibres resulted in a high pseudo-yield stress, but limited pseudo-ductile strain, while the earlier failure of the MR40 fibres provided a more balanced overall shape with a wide plateau and a lower pseudo-yield stress. This figure clearly shows that there is a trade-off between pseudo-ductile strain and pseudo-yield stress of the hybrid configurations and confirm the findings of our previous paper [44] presenting parametric studies of UD hybrid configurations based on an analytical model [43]. The G_{II} at the lower failure strain of the MR40 carbon fibres remained sub-critical even with a high relative carbon layer thickness resulting in a high initial modulus. On the other hand the initial modulus of the SG/T1000/SG type was lower because the outstanding (approx. 2.3%) failure strain of the T1000 fibres resulting in high G_{II} (according to Eq. (2)) limited the critical carbon ply thickness allowable for progressive failure by fragmentation and stable pull-out. This is also highlighted by the very limited absolute and relative thicknesses of the carbon layer allowable for pseudo-ductile failure modes on the corresponding damage-mode map (see the small coloured area in Fig. 2d).

The favourable pseudo-ductile stress–strain responses of the configurations comprising the highest modulus carbon fibres are presented in Fig. 7 and are in agreement with the predictions of Fig. 2e and f. The initial moduli of the S3G/M55/S3G and SG/$XN80_2$/SG type specimens were both outstanding and comparable to that of HS carbon/epoxy non-hybrid composites (113 and 124 GPa respectively). The relative carbon layer thickness and the carbon fibre modulus were higher for the XN80, but the difference in stiffness was reduced by the high volume fractions of the M55 and S3-glass fibres and the higher initial modulus of the S3-glass compared to the S-glass fibres. The pseudo-ductile failure mode area on Fig. 2e was limited by the relatively low failure strain of the S3-glass and the low G_{IIC} of this configuration. The first fracture of the XN80 carbon layer was early therefore the pseudo-yield stress was relatively low. On the other hand the pseudo-ductile strain was the highest (up to 2.6%) for this configuration. The S3G/M55/S3G type generated a more balanced stress–strain response with high initial modulus, yield stress and pseudo-ductile strain. However, the S3-glass fibre properties resulted in slightly lower final failure strain than that of the S-glass configurations, which limited the achievable pseudo-ductile strain. The set of graphs corresponding to the S3G/M55/S3G configuration on Fig. 6 show minor variation of the stress along the plateau, which corresponds to small load drops due to limited localised interfacial damage which appeared instantaneously after the carbon layer cracks. This is in agreement with the corresponding G_{II} = 0.328 N/mm relatively close to the critical value (0.5 N/mm for this material combination, see Table 3), which indicates that there is a small risk of delamination for this configuration. The less stable nature of the fragmentation and delamination process observed for the hybrids containing high modulus carbon might also be affected by the various dynamics of the fracture mechanisms depending on the stiffness ratio of the adjacent layers.

Table 4 summarises the results of the tested configurations and gives the definitions of the pseudo-ductility parameters. The initial modulus values were evaluated with the nominal thicknesses (see Table 3) and the pseudo-ductility parameters were determined graphically on the aggregated test graphs of each series. The table reveals, that the final failure strains of all hybrid configurations is significantly lower than the quoted failure strain of the S-glass fibres, but we have no information on how the fibre strain was measured. This effect is commonly observed in any type of UD composites and usually attributed to stress concentrations at the grips, size effects and possible manufacturing and machining defects.

The evaluated pseudo-ductile strains were in good agreement with those predicted by the damage mode maps. This is remarkable given that the prediction of the damage mode maps were largely based on constituent fibre properties from the manufacturers' datasheets and the approximate fracture toughness of the layer interfaces. The graphs of Figs. 4–7 as well as Table 4 highlight that the stress–strain response of the tested pseudo-ductile hybrid specimen configurations were strongly affected by the failure strain of the carbon layer. The observed damage modes ranged from well distributed multiple crack formation (fragmentation) to single catastrophic delamination at the first crack (for non-ductile, thicker TR30 carbon configurations). The most important trends identified for the pseudo-ductile configurations of the same

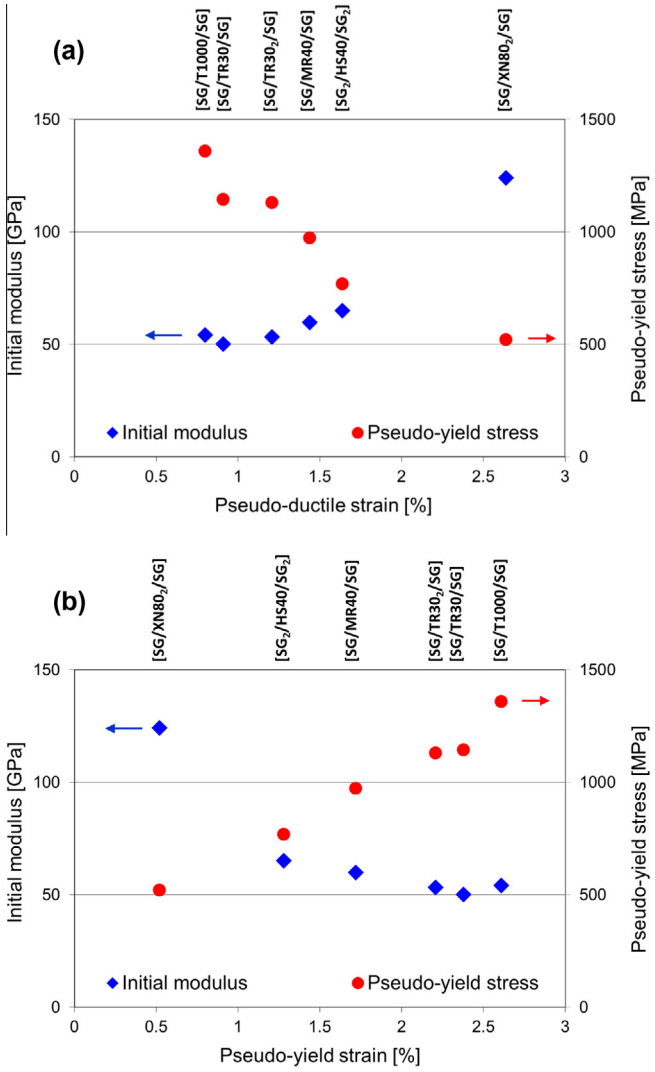

Fig. 8. Representation of the trends identified in the test data.

S-glass/epoxy high strain material hybridised with various carbon/epoxy low strain materials are presented in Fig. 8. Two groups of parameters were distinguished: (i) initial modulus and pseudo-ductile strain and (ii) pseudo-yield stress and strain, according to the similar trends they followed across the tested hybrid configurations. The correlations within the two groups are highlighted in the left axis plot of Fig. 8a and the right axis plot of Fig. 8b respectively. The right axis plot of Fig. 8a highlights the trade-off identified between the pseudo-ductile strains and the pseudo-yield stresses of the tested hybrids. The inverse correlation, found between the initial modulus and the pseudo-yield strain of the tested configurations, is shown in the left axis plot of Fig. 8b. This trend corresponds to the intrinsic trade-off between the tensile modulus and failure strain of different carbon fibre grades.

Moreover, the highest modulus XN80 fibres failed so early, that it was possible to suppress unstable delamination (because of the low G_{II} at low strains) even with thicker carbon layers (high relative carbon thickness), which improved the initial modulus of the UHM carbon hybrid further. These conditions resulted in outstanding initial modulus and high pseudo-ductile strain, but relatively low pseudo-yield strain and stress for the UHM carbon hybrid configuration. This configuration demonstrated that it is possible to combine the stiffness of high strength carbon and the final failure strain of S-glass composites.

The other extreme was the configuration comprising the highest failure strain T1000 carbon fibres, where late damage initiation resulted in high pseudo-yield strain and stress, but limited pseudo-ductile strain. Only a low carbon thickness was allowable for this specimen type because of the high G_{II} at the onset of damage in the carbon, therefore the initial modulus increase compared to the glass/epoxy baseline was moderate. The thinnest TR30 carbon plies allowed for a series of configurations illustrating the design flexibility in tuning the failure sequence and stress–strain response of UD thin-ply hybrids by changing the relative and the absolute carbon thickness in the specimen types.

4. Conclusions

The following conclusions were drawn from the extensive study of thin-ply unidirectional carbon/glass fibre reinforced epoxy interlayer hybrid composites:

- A range of new material combinations providing favourable pseudo-ductile stress–strain responses were developed using various thin carbon/epoxy and standard thickness S-glass/epoxy prepregs, suitable for tensile load dominated applications.
- The SG/XN80$_2$/SG configuration provided the combination of high initial modulus up to 124 GPa, similar to that of high strength carbon/epoxy and a final failure strain similar to that of S-glass/epoxy with a pseudo ductile strain of 2.64%.
- The SG/MR40/SG configuration demonstrated balanced properties of 60 GPa initial modulus, 970 MPa pseudo-yield stress and 1.44% pseudo-ductile strain.
- The strong correlation between the initial modulus and the pseudo-ductile strain was confirmed experimentally for the tested hybrid configurations and it was attributed to the trade-off between the failure strain and tensile modulus of the carbon fibre types.
- The trade-off between the achievable pseudo-ductile strain and the pseudo-yield stress was also confirmed experimentally as a key feature which governs the design of pseudo-ductile hybrid laminates.
- A two-step procedure was presented involving simple analytical criteria and the novel damage mode maps which were applied here for the first time for the design of unidirectional interlayer hybrid composites, assuring favourable pseudo-ductile failure through carbon layer fragmentation and stable pull-out.
- Good agreement was demonstrated between the analytically predicted and experimentally observed failure modes and pseudo-ductile strains. The damage mode maps based on basic mechanical properties of the constituent plies provided insight into the important factors for optimal hybrid configuration design.

Acknowledgements

This work was funded under the UK Engineering and Physical Sciences Research Council Programme Grant EP/I02946X/1 on High Performance Ductile Composite Technology in collaboration with Imperial College London. Gergely Czél acknowledges the Hungarian Academy of Sciences for funding through the Post-Doctoral Researcher Programme fellowship scheme, the János Bolyai scholarship and the Hungarian National Research, Development and Innovation Office (NKFIH) for funding through Grant Ref. K 116070. The authors acknowledge Hexcel Corporation and North TPT for supplying materials for this research. Supporting data can be requested from the corresponding author.

References

[1] Chawla KK. Composite materials: science and engineering. New York: Springer-Verlag; 2012.
[2] Mészáros L, Turcsán T. Development and mechanical properties of carbon fibre reinforced EP/VE hybrid composite systems. Periodica Polytech Mech Eng 2014;58:127–33.
[3] Boncel S, Rajyashree M, Sundaram RM, Windle AH, Koziol KKK. Enhancement of the mechanical properties of directly spun CNT fibers by chemical treatment. ACS Nano 2011;5:9339–44.
[4] Allaer K, De Baere I, Lava P, Van Paepegem W, Degrieck J. On the in-plane mechanical properties of stainless steel fibre reinforced ductile composites. Compos Sci Technol 2014;100:34–43.
[5] Callens MG, Gorbatikh L, Verpoest I. Ductile steel fibre composites with brittle and ductile matrices. Compos A Appl Sci Manuf 2014;61:235–44.
[6] Callens MG, Gorbatikh L, Bertels E, Goderis B, Smet M, Verpoest I. Tensile behaviour of stainless steel fibre/epoxy composites with modified adhesion. Compos A Appl Sci Manuf 2015;69:208–18.
[7] Callens MG, De Cuyper P, Gorbatikh L, Verpoest I. Effect of fibre architecture on the tensile and impact behaviour of ductile stainless steel fibre polypropylene composites. Compos Struct 2015;119:528–33.
[8] Fuller JD, Wisnom MR. Pseudo-ductility and damage suppression in thin ply CFRP angle-ply laminates. Compos A Appl Sci Manuf 2015;69:64–71.
[9] Fuller JD, Wisnom MR. Exploration of the potential for pseudo-ductility in thin ply CFRP angle-ply laminates via an analytical method. Compos Sci Technol 2015;112:8–15.
[10] Fuller JD, Jalalvand M, Wisnom MR. Combining fibre rotation and fragmentation to achieve pseudo-ductile CFRP laminates. Compos Struct 2016;142:155–66.
[11] Pimenta S, Robinson P. Wavy-ply sandwich with composite skins and crushable core for ductility and energy absorption. Compos Struct 2014;104:111–24.
[12] Qiana H, Bismarck A, Greenhalgh ES, Shaffer MSP. Carbon nanotube grafted carbon fibres: a study of wetting and fibre fragmentation. Compos A Appl Sci Manuf 2010;41:1107–14.
[13] Grail G, Pimenta S, Pinho ST, Robinson P. Exploring the potential of interleaving to delay catastrophic failure in unidirectional composites under tensile loading. Compos Sci Technol 2015;106:100–9.
[14] Pimenta S, Robinson P. An analytical shear-lag model for composites with 'brick-and-mortar' architecture considering non-linear matrix response and failure. Compos Sci Technol 2014;104:111–24.
[15] Czel G, Pimenta S, Wisnom MR, Robinson P. Demonstration of pseudo-ductility in unidirectional discontinuous carbon fibre/epoxy prepreg composites. Compos Sci Technol 2015;106:110–9.
[16] Hancox NL. Fibre composite hybrid materials. London: Applied Science Publishers Ltd.; 1981.
[17] Summerscales J, Short D. Carbon fibre and glass fibre hybrid reinforced plastics. Composites 1978;9:157–66.
[18] Short D, Summerscales J. Hybrids – a review Part 1. Techniques design and construction. Composites 1979;10:215–21.
[19] Short D, Summerscales J. Hybrids – a review Part 2. Physical properties. Composites 1980;11:33–8.
[20] Kretsis G. A review of the tensile, compressive, flexural and shear properties of hybrid fibre-reinforced plastics. Composites 1987;18:13–23.
[21] Hayashi T. Development of new material properties by hybrid composition. 1st report. Fukugo Zairyo (Compos Mater) 1972;1:18–20.
[22] Hayashi T, Koyama K, Yamazaki A, Kihira M. Development of new material properties by hybrid composition. 2nd report. Fukugo Zairyo (Compos Mater) 1972;1:21–5.
[23] Bunsell AR, Harris B. Hybrid carbon and glass fibre composites. Composites 1974;5:157–64.
[24] Manders PW, Bader MG. The strength of hybrid glass/carbon fibre composites. J Mater Sci 1981;16:2233–45.
[25] Marom G, Fischer S, Tuler FR, Wagner HD. Hybrid effects in composites: conditions for positive or negative effects versus rule-of-mixtures behaviour. J Mater Sci 1978;13(7):1419–26.
[26] Svensson N. Manufacturing of thermoplastic composites from commingled yarns – a review. J Thermoplast Compos Mater 1998;11(1):22–56.
[27] Swolfs Y, Gorbatikh L, Verpoest I. Fibre hybridisation in polymer composites: a review. Compos A Appl Sci Manuf 2014;67:181–200.
[28] Diao H, Bismarck A, Robinson P, Wisnom MR. Pseudo-ductile behaviour of unidirectional fibre reinforced polyamide-12 composite by intra-tow hybridization. In: Proceedings of ECCM 15 conference. Venice; June 2012.
[29] Yu H, Wisnom MR, Potter KD. A novel manufacturing method for aligned discontinuous fibre composites (high performance-discontinuous fibre method). Compos A Appl Sci Manuf 2014;65:175–85.
[30] Yu H, Longana ML, Jalalvand M, Wisnom MR, Potter KD. Pseudo-ductility in intermingled carbon/glass hybrid composites with highly aligned discontinuous fibres. Compos A Appl Sci Manuf 2015;73:35–44.
[31] Czél G, Wisnom MR. Demonstration of pseudo-ductility in high performance glass–epoxy composites by hybridisation with thin-ply carbon prepreg. Compos A Appl Sci Manuf 2013;52:23–30.
[32] Jalalvand M, Czél G, Wisnom MR. Numerical modelling of the damage modes in UD thin carbon/glass hybrid laminates. Compos Sci Technol 2014;94:39–47.
[33] Sihn S, Kim RY, Kawabe K, Tsai SW. Experimental studies of thin-ply laminated composites. Compos Sci Technol 2007;67:996–1008.
[34] Yokozeki T, Aoki Y, Ogasawara T. Experimental characterization of strength and damage resistance properties of thin-ply carbon fiber/toughened epoxy laminates. Compos Struct 2008;82:382–9.
[35] Yokozeki T, Kuroda A, Yoshimura A, Ogasawara T, Aoki T. Damage characterization in thin-ply composite laminates under out-of-plane transverse loadings. Compos Sci Technol 2010;93:49–57.
[36] Saito H, Morita M, Kawabe K, Kanesaki M, Takeuchi H, Tanaka M, et al. Effect of ply-thickness on impact damage morphology in CFRP laminates. J Reinf Plast Compos 2011;30:1097–106.
[37] Arteiro A, Catalanotti G, Xavier J, Camanho PP. Notched response of non-crimp fabric thin-ply laminates. Compos Sci Technol 2013;79:97–114.
[38] Arteiro A, Catalanotti G, Xavier J, Camanho PP. Notched response of non-crimp fabric thin-ply laminates: analysis methods. Compos Sci Technol 2013;88:165–71.
[39] Amacher R, Cugnoni J, Botsis J, Sorensen L, Smith W, Dransfeld C. Thin ply composites: experimental characterization and modeling of size-effects. Compos Sci Technol 2014;101:121–32.
[40] Guillamet G, Turon A, Costa J, Renart J, Linde P, Mayugo JA. Damage occurrence at edges of non-crimp-fabric thin-ply laminates under off-axis uniaxial loading. Compos Sci Technol 2014;98:44–50.
[41] Borg C. An introduction to spread tow reinforcements: Part 1 – manufacture and properties. Reinf Plast 2015;59:194–8.
[42] Ohlsson F. An introduction to spread tow reinforcements. Part 2: design and applications. Reinf Plast 2015;59:228–32.
[43] Jalalvand M, Czél G, Wisnom MR. Damage analysis of pseudo-ductile thin-ply UD hybrid composites – a new analytical method. Compos A Appl Sci Manuf 2015;69:83–93.
[44] Jalalvand M, Czél G, Wisnom MR. Parametric study of failure mechanisms and optimal configurations of pseudo-ductile thin-ply UD hybrid composites. Compos A Appl Sci Manuf 2015;74:123–31.
[45] Czél G, Jalalvand M, Wisnom MR. Demonstration of pseudo-ductility in unidirectional hybrid composites made of discontinuous carbon/epoxy and continuous glass/epoxy plies. Compos A Appl Sci Manuf 2015;72:75–84.
[46] Czél G, Jalalvand M, Wisnom MR. Development of pseudo-ductile hybrid composites with discontinuous carbon- and continuous glass prepregs. In: Proceedings of ECCM-16 conference. Seville; June 2014.
[47] Wisnom MR, Czel G, Swolfs Y, Jalalvand M, Gorbatikh L, Verpoest I. Hybrid effects in thin ply carbon/glass unidirectional laminates: accurate experimental determination and prediction. Compos A Appl Sci Manuf; in press.